Large spin-orbit-torque efficiency and room-temperature magnetization switching in SrIrO₃/Co-Fe-B heterostructures

Peng Li, ^{1,2}, * Sanyum Channa, ^{1,2} Xiang Li, ^{3,4} Laith Alahmed, ⁵ Chunli Tang, ⁵ Di Yi, ¹ Lauren Riddiford, ^{1,2} Jacob Wisser, ^{1,2} Purnima P. Balakrishnan, ^{1,6} Xin Yu Zheng, ^{1,2} Di Lu, ⁷ Arturas Vailionis, ^{8,9} Shan X. Wang, ^{3,4} and Yuri Suzuki^{1,2} ¹ Geballe Laboratory of Advanced Materials, Stanford University, Stanford, California 94305, USA

² Department of Applied Physics, Stanford University, Stanford, CA 94305, USA

³ Department of Electrical Engineering, Stanford University, Stanford, California 94305, USA

⁴ Department of Materials Science and Engineering, Stanford University, Stanford, California 94305, USA

⁵ Department of Electrical and Computer Engineering, Auburn University, Auburn, AL 36849

⁶ Department of Physics, Stanford University, Stanford, CA 94305, USA

⁷ School of Microelectronics, University of Science and Technology of China, Hefei 230052, China

⁸ Stanford Nano Shared Facilities, Stanford University, Stanford, California 94305, USA

⁹ Department of Physics, Kaunas University of Technology, Kaunas, Lithuania

Spin-orbit torque switching (SOT) is a potentially energy efficient mechanism by which electrical current can control magnetization. We demonstrate room temperature spin-orbit torque switching in nanometer thick CoFeB/SrIrO₃ bilayers despite the amorphous nature of CoFeB and the interface. This behavior is attributed to the large spin Hall angle in SrIrO₃ as well as high spin transmission at the interface that contribute to the spin-orbit-torque efficiency ξ_{SOT} . Our bilayers exhibit large ξ_{SOT} of up to 1.4 and effective spin Hall conductivity of 0.9×10^5 ($\hbar/2e$) Ω^{-1} m⁻¹. In our bilayers, we observe unidirectional magnetoresistance and current-induced magnetization switching with a low critical current density of 1.38×10^{10} A/m² at room temperature. Our results are promising for heterostructures combining technologically relevant CoFeB with high spin-orbit coupling oxides.

Introduction—Efficient electrical current switching of magnetization has been studied extensively to understand interactions between the charge and spin degrees of freedom but also to incorporate spin functionality into microelectronics. Current-induced switching of magnetization was theoretically predicted in the form of spin transfer torque by Slonzewski in 1996 [1], followed by the experiment of spin transfer torque (STT) switching in Co/Cu multilayer films[2, 3]. These experiments relied on spin polarized charge current with a high current density to generate STT to switch magnetization [1, 4]. More recent studies have focused on utilizing the spin Hall effect in high spin-orbit coupled materials to generate spin-orbit torques (SOT) [5–15]. In these studies, spin current is generated and injected into a neighboring ferromagnet to switch its magnetization. The selection of the spin-orbit coupled materials thus becomes critical for realizing low-current, low-power SOT switching.

Among the strongly spin-orbit coupled materials, 5d transition metal oxides have been identified as promising candidates and exhibit a range of exotic electronic and magnetic behavior [16–23]. A few studies have explored charge-spin conversion in SrIrO $_3$. It has been predicted that a large intrinsic spin Hall effect (SHE), hence large charge-to-spin conversion, arises in SrIrO $_3$ due to the Berry curvature from the nearly degenerate electronic spectra surrounding the nodal line [24]. Following the prediction, a handful of studies explored SrIrO $_3$ heterostructures with ferromagnetic metals such as permalloy [25–27], La $_{0.7}$ Sr $_{0.3}$ MnO $_3$ [28, 29] and SrRuO $_3$ [30].

These experiments demonstrated the SOT efficiency (ξ_{SOT}) , which is the figure of merit for charge-to spin conversion, to have values between 0.4 and 1.1 for SrIrO₃.

To date, SOT switching has been demonstrated in epitaxial SrIrO₃-based heterostructures with SrRuO₃ and more recently La_{0.7}Sr_{0.3}MnO₃. Since current flows through both the ferromagnetic and non-magnetic layers, it is difficult to deduce an accurate critical current density for magnetization switching. However epitaxial SrIrO₃/SrRuO₃ heterostructures are estimated to have a critical current density of $4.6 - 5.0 \times 10^{10} \text{ A/m}^2$ at 70 K [30]. These studies demonstrate the potential for SrIrO₃ in SOT device applications. More recently room-temperature current-induced SOT switching using SrIrO₃ has been shown in SrIrO₃/La_{0.7}Sr_{0.3}MnO₃ heterostructures but without any estimate of a critical current density for switching [31]. In order for SrIrO₃ to be technologically viable, it is essential to study heterostructures with CoFeB which is the ferromagnetic material of choice in modern magnetic memory. [32, 33] CoFeB with its perpendicular magnetic anisotropy provides higher speed, energy efficiency and density as well as better endurance for magnetic random-access memory devices.

In this paper, we report the demonstration of current-induced SOT magnetization switching in $CoFeB/SrIrO_3$ heterostructures at room temperature and the critical factors governing its manifestation. These heterostructures are composed of amorphous CoFeB layers deposited on an epitaxial $SrIrO_3$ films. From spin-torque ferromagnetic resonance (ST-FMR) measurements, we de-

duced a large ξ_{SOT} of up to 1.4 in our bilayers. The large ξ_{SOT} is further confirmed by second harmonic resistance measurements. Assuming a SrIrO₃ conductivity in bilayers similar to that in single layers of SrIrO₃, we deduced high spin Hall conductivity values of 0.9×10^5 $(\hbar/2e)\Omega^{-1}m^{-1}$, which are similar to Pt. We detected unidirectional magnetoresistance (UMR) in our bilayers, indicating a spin-dependent interface resistance attributed to current-induced spin accumulation. By monitoring the UMR in our second harmonic measurements, we demonstrated current-induced magnetization switching at room temperature with an estimated critical current density of $1.38 \times 10^{10} \text{ A/m}^2$ in the absence of any magnetic field. Despite the amorphous nature of the ferromagnetic CoFeB layer and the interface, we observe lower critical current densities than previously demonstrated in analogous systems, such as an epitaxial SrRuO₃/SrIrO₃ heterostructure at 70 K [30]. Together our results demonstrate the promise of high spin-orbit coupled oxide layers as charge-to-spin converters in technologically relevant CoFeB-based heterostrucures.

Results-We synthesized a series of heterostructures of CoFeB $(t_{\rm M}=3, 5 \text{ nm})/\text{SrIrO}_3$ $(t_{\rm SIO}=4-13 \text{ nm})$ on (100) (LaAlO₃)_{0.3} (Sr₂AlTaO₆)_{0.7} (LSAT) substrates and capped with a 1.5 nm Ta/2 nm MgO bilayer. Single layer films of SrIrO₃ and CoFeB were also deposited on (100) LSAT substrates for reference. The SrIrO₃ layer was grown in a pulsed laser deposition chamber and then transferred to a sputtering chamber for the deposition of the CoFeB layer (see Supplement) [34]. The surface morphology of the heterostructures was measured with a Bruker Digital 3100 atomic force microscope. In order to assess crystalline structure and film thickness, xray diffraction and x-ray reflectivity measurements were performed on a PANalytical X'Pert Materials Research Diffractometer at the Stanford Nano Shared Facilities. These measurements were complemented by synchrotron XRD at the Stanford Synchrotron Radiation Laboratory (SSRL) at SLAC National Accelerator Laboratory. The temperature and magnetic field dependence of the magnetization in the samples were measured with a Quantum Design Magnetic Property Measurement System. ST-FMR measurements were performed on a home built FMR system. The electrical measurements were conducted with a Quantum Design PPMS Dynacool system supplemented with two SR830 lock-in-amplifiers and a Keithley 6221 AC and DC current source.

In our bilayers, we found the CoFeB layers to grow as amorphous layers on highly crystalline epitaxial $SrIrO_3$ layers on LSAT (001) substrates. The structure of the $SrIrO_3/LSAT(001)$ thin films was studied using high-resolution x-ray diffraction at SSRL. Fig.1a shows symmetrical x-ray diffraction profiles around the $SrIrO_3(002)_{pc}$ Bragg peak for two $SrIrO_3$ layers of different thicknesses. The observed strong Laue oscillations around the main $SrIrO_3(002)_{pc}$ peaks indicate high crys-

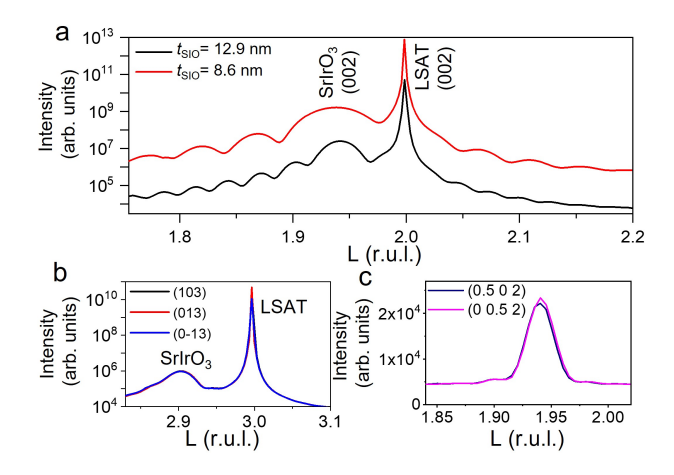


FIG. 1. High resolution synchrotron X-ray characterization of SrIrO₃/LSAT samples. (a) X-ray diffraction spectra showing the (002) peaks of SrIrO₃ and LSAT substrate for t_{SIO} = 12.9 nm and 8.6 nm, respectively. (b) Asymmetric (103) $_{pc}$, (013) $_{pc}$, and (0-13) $_{pc}$ diffraction peaks for the 12.9 nm SrIrO₃ sample. (c) Half-order Bragg peaks (0.5 0 2) and (0 0.5 2) for a 12.9 nm SrIrO₃ sample.

talline order throughout the whole film thickness. The symmetrical scans over a wider range of 2θ showed only $(00l)_{pc}$ -type of SrIrO₃ peaks. The c/a ratio of the pseudocubic unit cell was calculated from $(002)_{pc}$ and $(103)_{pc}$ Bragg peak positions shown in Fig. 1a and 1b. For 12.9 nm SrIrO₃, the c/a ratio was estimated to be 1.031 signifying a compressive strain of the SrIrO₃ lattice on the LSAT(001) substrate. Differences in the positions of asymmetric $(103)_{pc}$, $(013)_{pc}$, and $(0-13)_{pc}$ Bragg peaks would be consistent with an orthorhombic unit cell with [110]_o out-of-plane orientation. In our samples, overlapping $(103)_{pc}$, $(013)_{pc}$ and $(0-13)_{pc}$ Bragg peaks (Fig. 1b) suggests a tetragonal unit cell. However we also observe $(0.5 \ 0 \ 2)_{\rm pc}$ and $(0 \ 0.5 \ 2)_{\rm pc}$ peaks, which are forbidden in a tetragonal unit cell. The (0.5 0 2)_{pc} peaks of the pseudo-cubic unit cell correspond to the (221)_o peaks of the orthorhombic unit cell that are caused by the a⁺b⁻c⁻ octahedral rotation pattern and their origin is attributed to the slight displacement of Sr cations in the SrIrO₃ unit cell[35]. The presence of the (221)_o peaks unequivocally indicates an orthorhombic unit cell with $a_o \approx b_o$ that is oriented $[110]_{\rm o}$ out-of-plane. As can be seen from Fig. 1c, both of these peaks are present with the same intensities, indicating 90° twins of the SrIrO₃ [110]₀ oriented orthorhombic unit cells with a 50%-50% ratio along LSAT[100] and [010] directions. Such a twin-domain ratio should effectively suppress any anisotropy in the SOT efficiency in the in-plane crystallographic orientation.

ST-FMR measurements of CoFeB $(5 \text{ nm})/\text{SrIrO}_3$ (4.3 -12.9 nm)/LSAT samples indicate large spin-torque efficiencies compared with previous studies [25–27, 29, 30]. As shown in Fig. 2a, the samples were patterned into

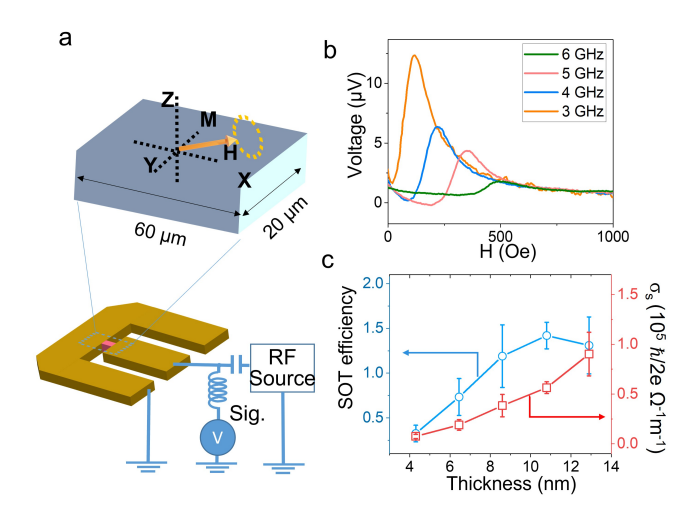


FIG. 2. Characterization of charge-to-spin conversion in SrIrO₃/LSAT samples. (a) Schematic of ST-FMR experiment. (b) ST-FMR voltage vs. magnetic field for a CoFeB (5 nm)/SrIrO₃ (12.9 nm) sample at 3-6 GHz. (c) Dependence of SOT efficiency ($\xi_{\rm SOT}$) and effective spin Hall conductivity ($\sigma_{\rm s}^{\rm eff}$) on the SrIrO₃ thickness.

60 μ m \times 10 μ m strips. On the same sample, multiple ST-FMR patterns were fabricated with the long-axis of the strips aligned along the $\langle 100 \rangle$, $\langle 001 \rangle$ and $\langle 110 \rangle$ directions of SrIrO₃. We deduced the SOT efficiency ξ_{SOT} , which is a product of the spin Hall angle and the interfacial spin transparency, in different in-plane directions. These strips were contacted with Ti (10 nm)/Au (120 nm) coplanar waveguide patterns for microwave input and signal detection. ξ_{SOT} is estimated from the ST-FMR lineshape through the ratio of the symmetric and asymmetric Lorentzian functions and plotted in Fig. 2c.[36] The ST-FMR lineshapes were fitted for a range of magnetic field windows to minimize overestimation of $\xi_{\rm SOT}$. We also measured the conductivity σ of SrIrO₃ films and plotted effective spin Hall conductivity $\sigma_{\rm s}^{\rm eff}$ which is comprised of the product of the ξ_{SOT} and σ of the SrIrO₃ layer. Overall both ξ_{SOT} and σ_s show an increasing trend with the $SrIrO_3$ thickness, taking into account the increased noise in the 12.9 nm sample. The maximal $\xi_{\text{SOT}} = 1.4$ value is comparable to the highest value measured in the La_{0.7}Sr_{0.3}MnO₃/SrIrO₃ system, which has a lattice-matched, epitaxial interface [29]. However, the CoFeB/SrIrO₃ system suggests that an amorphous ferromagnetic layer or interface does not preclude efficient charge-to-spin conversion.

We performed ac magnetoresistance measurements to extract UMR and demonstrate SOT switching. The films were patterned into 10 μ m wide Hall bar devices. Fig. 3a and 3b show the configurations of resistivity measurements. The results presented in Fig. 3c-d are at an ac current of 0.6 mA. The first harmonic Hall resistance $R_{\text{xy-}1\omega}$ shows a typical planar Hall effect (see Supple-

ment) [34], while the second harmonic Hall resistance $R_{xy-2\omega}$ vs. angle exhibits a sinusoidal curve with a period of 360°. $R_{xy-2\omega}$ can be understood in terms of a dampinglike $(R_{\rm DL})$ torque, a field-like $(R_{\rm FL})$ torque and thermal contributions $(R_{\Delta T})$ from the anomalous Nernst effect (ANE) and spin Seebeck effect (SSE). The $R_{\rm FL}$ term follows a $\cos(2\phi)\cos(\phi)$ dependence while $R_{\rm DL}+R_{\Delta T}$ are proportional to $\cos(\phi)$ [37, 38]. The curves in Fig. 3c are well fit by $\cos(\phi)$, indicating that $R_{xy-2\omega}$ is comprised of damping-like torque and the thermal effects. To separate $R_{\rm DL}$ from $R_{\Delta T}$, we plot $R_{\rm xv-2\omega}$ as a function of inverse of the in-plane effective magnetic field $1/(H+H_{demag}-H_k)$ where H_{demag} is the demagnetization field and H_k is the anisotropy field (≈ 0) (Fig. 3e). The intercept of this plot is $R_{\Delta T}$ and here we deduce it to be 3.1 m Ω . The damping-like field is proportional to the slope of the curve and is estimated to be $H_{DL}=2$ Oe from $H_{\rm DL}$ =2Slope/ $R_{\rm AHE}$ [39] where $R_{\rm AHE}$ is the anomalous Hall resistance. This corresponds to a ξ_{SOT} of 1.3 for the 10.8 nm SrIrO₃, which is similar to that deduced from ST-FMR. Similar procedures can be used to extract $H_{\rm FL}+H_{\rm Oe}$ [39], suggesting that $H_{\rm Oe}$ is negligible in the system (see supplement)[34].

The second harmonic longitudinal resistance $R_{xx-2\omega}$ shows a sinusoidal dependence. A sinusoidal dependence can be indicative of UMR which is a spin-dependent interface resistance attributed to current-induced spin accumulation [40]. It should be noted that thermal resistances $R_{\Delta T}$ attributed to SSE and ANE can be mixed into $R_{xx-2\omega}$. To estimate their contributions, we estimate the thermal resistance measured from R_{xy} and scale it to the device length of the Hall bar. In this way, $R_{\rm UMR}$ can be separated from $R_{\Delta T}$ in $R_{xx-2\omega}$. The sinusoidal dependence of the second harmonic resistance $R_{\text{xx-}2\omega}$ in dicates that the Oersted field contributions are negligible as Fig. 3(d) can be well fit with a simple sinusoidal dependence. The total second harmonic longitudinal resistance $R_{\text{xx-}2\omega}$, R_{UMR} , and $R_{\Delta \text{T}}$ are plotted as a function of SrIrO₃ thickness in Fig. 3(e). As a function of SrIrO₃ thickness, the total $R_{xx-2\omega}$ exhibits non-monotonic behavior (Fig. 3e). The contribution from $R_{\Delta T}$ decreases with increasing SrIrO₃ thickness likely due to the overall decreasing resistance as SrIrO₃ becomes thicker. The non-monotonic trend in $R_{\rm UMR}$ can be explained in the following way: $R_{\rm UMR}$ increases up to 6nm of SrIrO₃ from spin accumulation at the CoFeB/SrIrO₃ interface; as the SrIrO₃ layer becomes thicker, more current flows in SrIrO₃ and less current is scattered at the CoFeB/SrIrO₃ interface, thus decreasing gradually R_{UMR} with increasing SrIrO₃ thickness. From the SrIrO₃ thickness dependence of UMR [40], we have estimated a spin diffusion length in SrIrO₃ of 2-3 nm that is consistent with previous results [25].

To demonstrate all-electrical switching of magnetization with large spin orbit torques from SrIrO₃, we fabricated a 40 μ m×10 μ m Hall bar from a

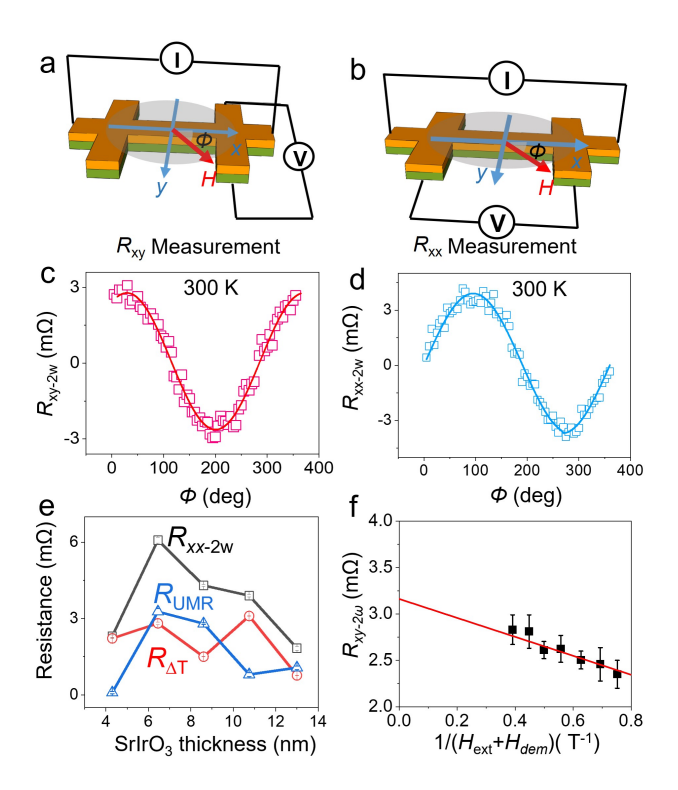


FIG. 3. Second harmonic resistance in CoFeB (5 nm)/SrIrO₃(10.8 nm) sample: (a) Schematic of angular measurement of $R_{\rm xy}$. (b) Schematic of angular measurement of $R_{\rm xx}$. (c) Angular dependence of $R_{\rm xy-2\omega}$ at 300K. The data points are fitted with $\cos(\phi)$. (d) Angular dependence of $R_{\rm xx-2\omega}$ at 300K and fit. (e) $R_{\rm xx-2\omega}$, $R_{\rm UMR}$, and $R_{\Delta \rm T}$ vs. SrIrO₃ thickness, respectively. (f) $R_{\rm xy-2\omega}$ as a function of the inverse of the in-plane effective magnetic field. ϕ is the angle between the field and the X-axis.

CoFeB(3nm)/SrIrO₃(10.8 nm) bilayer. To confirm magnetization switching, we monitor the UMR signal. The 10.8 nm thick SrIrO₃ film provides both large ξ_{SOT} and decent R_{UMR} signal while a uniform film with in-plane anisotropy can be achieved in 3 nm of CoFeB. Fig. 4a and b show a sketch of the measurement setup and the current waveforms, respectively. A 5 ms long d.c. pulse generates a damping-like torque that switches the magnetization along the y-axis while an a.c. current of 0.6 mA is used to monitor $R_{2\omega-xx}$ and detect the magnetization direction after a 20 s delay. As a reference, $R_{2\omega-xx}$ is measured as a function of magnetic field H along the y-axis showing magnetization and indicates that $R_{2\omega-xx}$ is switched by an in-plane magnetic field of $H_c=\pm 10$ Oe from $\pm 2 \text{ m}\Omega$. We then measured $R_{2\omega-xx}$ as a function of d.c. current pulse. In Fig. 4d, each data point represents the $R_{2\omega-xx}$ value after a dc pulse was applied. The arrows indicate the pulse sweeping directions. $I_{\rm dc}$ pulses switch the magnetization completely in the CoFeB film along the y axis, reaching $\pm 2 \text{ m}\Omega$ at large positive and negative d.c. pulse currents, respectively. Assuming that the current flows through the CoFeB and SrIrO₃ lay-

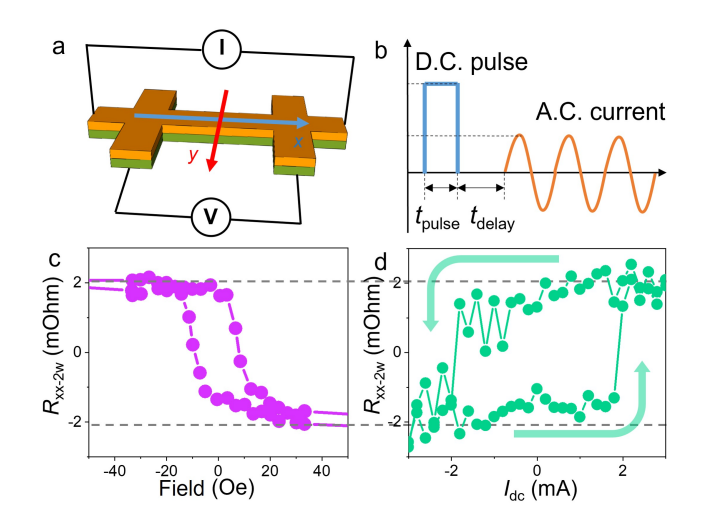


FIG. 4. Room-temperature Magnetization switching in CoFeB(3 nm)/SrIrO₃(10.8 nm). a, Cartoon showing the sample and measurement setup. The red line indicates the Y-axis of magnetization switching. b, Sequence for pulse d.c. and a.c currents. The d.c current is for generating spin-orbit torque for switching and the a.c. current is for reading the magnetization state. c, $R_{2\text{w-xx}}$ vs. the magnetic field along the y-axis showing magnetic field-induced magnetization switching. d, $R_{2\text{w-xx}}$ measured as a function of pulse current amplitude I_{dc} at zero external fields.

ers like parallel resistors, we calculated a critical current density of 1.38×10¹⁰ A/m² which is about one order of magnitude lower than using a heavy metal such as Pt. It should be noted that we assumed resistivity values from single layers of CoFeB and SrIrO₃ in our calculations of the bilayers. At room temperature, the resistivity values of the SrIrO₃ and CoFeB layers are 2.61 m Ω ·cm and 2.3 m Ω ·cm respectively. This may not be an accurate assumption since the nature of CoFeB grown on SrIrO₃ (in contrast to grown directly on the substrate) may alter the resistivity values and the interface resistance is also ignored. The Oersted field due to the applied current is estimated to be around 1 Oe which is 10% of the coercivity of the sample. Measurements with a range of a.c. current values as well as wait times between the d.c. pulse and a.c. measure current show no indication of heating effects. Thus we have demonstrated all-electrical current magnetization switching with a very low current density at room temperature.

SOT structure	$\xi_{ ext{SOT}}$	$\sigma(\Omega^{-1}\mathrm{m}^{-1})$	$\sigma_{\rm A}^{eff}(\hbar/2e\Omega^{-1}{\rm m}^{-2})$
SrIrO ₃ (12.9 nm)/CoFeB	1.31	6.7×10^4	0.9×10^{5}
$SrIrO_3/LSMO[29]$	1.5	-	$(1-3)\times10^5$
Pt/NiFe[41]	0.08	-	3.4×10^{5}
Pt/MAFO[42]	0.14	-	6×10^{5}
$Bi_2Se_3/NiFe[43]$	2 - 3.5	-	$(1.1-2)\times10^5$

TABLE I. SOT efficiency, conductivity σ and effective spin Hall conductivity $\sigma_{\rm A}^{\rm eff}$ of SOC overlayers.

To date, there have only been a handful of studies that deduce SOT efficiencies of SrIrO₃ [25–27]. SOT generation and switching studies based on SrIrO₃ have involved all-oxide epitaxial heterostructures, such as $SrRuO_3/SrIrO_3[30]$ and $La_{0.7}Sr_{0.3}MnO_3/SrIrO_3$ bilayers [29, 31], as well as polycrstalline bilayers, such as $NiFe/SrIrO_3$ [27]. One might expect that epitaxial bilayers with coherent interfaces should have the largest charge-spin conversion efficiency with superior interface spin transparency. Epitaxial bilayers of La_{0.7}Sr_{0.3}MnO₃/SrIrO₃ have been shown to exhibit SOT efficiencies on the order of 1. On oxide spinels, even Pt has been shown to grow epitaxially on oxides and give rise to large SOT efficiencies [42]. More relevantly, polycrystalline bilayers have shown SOT efficiencies of up to 1.1 with SOT efficiency values increasing with increasing SrIrO₃ thickness[26]. These results suggest that a structurally coherent interface is not a critical factor in maximizing SOT efficiency. SOT efficiency is a product of the spin Hall angle of the non-magnetic material and spin transparency of the interface with the spin Hall angle has been shown to be higher for higher resistance material (e.g., induced by impurity doping [31]). Since the resistivity of SrIrO₃ is significantly higher than Pt but lower than Bi₂Se₃, the high SOT efficiency found in our $SrIrO_3$ is not too surprising.

In the case of our CoFeB/SrIrO₃ bilayers, we observe a SOT efficiency that is as high as 1.4. This SOT efficiency includes not only the intrinsic and extrinsic contribution to the charge-to-spin conversion from the bulk of the SrIrO₃ layer but also an interface spin transparency contribution. The amorphous interface may give rise to an interdiffused layer at the interface that can induce strong electron scattering, thus affecting the overall SOT efficiency [44–46]. However the SOT efficiency values in our bilayers would suggest that coherent interfaces are not critical in obtaining large SOT efficiencies.

In fact, although La_{0.7}Sr_{0.3}MnO₃/SrIrO₃ bilayers exhibit spin-orbit torque efficiencies almost as large as our CoFeB/SrIrO₃ bilayers, recent results in La_{0.7}Sr_{0.3}MnO₃/SrIrO₃ [31] bilayers, where room temperature current-induced magnetization switching has been observed, show damping -like torque efficiencies of 0.15. The only other epitaxial SrIrO₃ based system that has exhibited SOT switching is the SrRuO₃/SrIrO₃ bilayer [30]. In this epitaxial bilayer, the SOT efficiency is also significantly lower between 0.58 and 0.86 and is limited to 70 K, likely due to the low T_c of SrRuO₃. Our results show that SOT efficiency depends critically on the crystallinity and high atomic spin-orbit coupling of the SrIrO₃ or equivalent layer, but is robust to the presence of disorder in the ferromagnet or at the interface.

As a point of comparison, previous studies of β -W/CoFeB spin-orbit torque devices exhibit SOT efficincies on the order of 0.4 compared to 1.4 in our devices [47]. Switching current density $(1.38 \times 10^{10} \text{ A/m}^2)$ in

our devices are an order of magnitude lower than that for β -W/CoFeB (10¹¹ A/m²)[48]. This is not too surprising since by definition SOT efficiency is proportional to resistivity. Hence more resistive materials such as SrIrO₃ and even Bi₂Se₃ generally show higher SOT efficiencies. Moreover, the different phases of W limits the thicknesses for which the pure β -W phase can be stabilized. Other candidates for the spin-to-charge conversion layer such as Pt have significantly smaller SOT efficiencies in heterostructures with CoFeB. In previous work on NiFe/SrIrO₃, large SOT efficiency of 0.4 was measured but SOT-induced magnetization switching was not demonstrated in NiFe/SrIrO₃ heterostructures. Therefore our demonstration of SOT-induced magnetization switching at room temperature in CoFeB/SrIrO₃ is a significant advance.

summary, have demonstrated we temperature current-induced magnetization switching in CoFeB/SrIrO₃ bilayers at low critical current densities. Spin torque ferromagnetic measurements have enabled us to deduce SOT efficiency as large as 1.4. monitoring of the SOT magnetization switching through the unidirectional magnetoresistance (UMR) signal has demonstrated room temperature SOT switching at critical current densities significantly lower than previously observed. This system demonstrates the critical factors of crystallinity and high spin-orbit coupling in the charge-to-spin conversion layer and the robustness of SOT switching to the presence of disorder in the ferromagnet and the interface. The high SOT efficiency, large signal-to-noise and low switching current density provide an ideal platform to optimize SOT switching performance and realize next-generation spin-orbit torque based MRAM devices.

Acknowledgements-This work was supported by the National Science Foundation on Award DMR-2037652. L.J.R. was supported by the Air Force Office of Scientific Research and an NSF Graduate Research Fellowship. X.Y.Z. was also supported on U.S. Department of Energy, Director, Office of Science, Office of Basic Energy Sciences, Division of Materials Sciences and Engineering under Contract No. DESC0008505. Use of the Stanford Synchrotron Radiation Light source, SLAC National Accelerator Laboratory, is supported by the U.S. Department of Energy, Office of Science, Office of Basic Energy Sciences under Contract No. DE-AC02-76SF00515. The Advanced Light Source is supported by the Director, Office of Science, Office of Basic Energy Sciences, of the U.S. Department of Energy under Contract No. DE-AC02-05CH11231. Use of the Advanced Photon Source was supported by the U. S. Department of Energy, Office of Science, Office of Basic Energy Sciences, under Contract No. DE-AC02-06CH11357. Part of this work was performed at the Stanford Nano Shared Facilities (SNSF), supported by the National Science Foundation

under award ECCS-2026822. P.L. acknowledges the discussions with Prof. Tianxiang Nan and Dr. Mahendra DC.

- * lipeng18@ustc.edu.cn
- J. C. Slonczewski, Current-driven excitation of magnetic multilayers, J. Magn. Magn. Mater. 159, L1 (1996).
- [2] M. Tsoi, A. G. M. Jansen, J. Bass, W.-C. Chiang, M. Seck, V. Tsoi, and P. Wyder, Excitation of a magnetic multilayer by an electric current, Phys. Rev. Lett. 80, 4281 (1998).
- [3] D.C. Ralph and M.D. Stiles, Spin transfer torques, J. Magn. Magn. Mater. 320, 1190 (2008).
- [4] L. Berger, Emission of spin waves by a magnetic multilayer traversed by a current, Phys. Rev. B 54, 9353 (1996).
- [5] Luqiao Liu, O. J. Lee, T. J. Gudmundsen, D. C. Ralph, and R. A. Buhrman, Current-induced switching of perpendicularly magnetized magnetic layers using spin torque from the spin Hall effect, Phys. Rev. Lett. 109, 096602 (2012).
- [6] L. Liu, C.-F. Pai, Y. Li, H. W. Tseng, D. C. Ralph, and R. A. Buhrman, Spin-torque switching with the giant spin Hall effect of tantalum, Science 336, 555 (2012).
- [7] S. Emori, U. Bauer, S.-M. Ahn, E. Martinez, and G. S. D. Beach, Current-driven dynamics of chiral ferromagnetic domain walls, Nat. Mater. 12, 611 (2013).
- [8] R. Lo Conte, A. Hrabec, A. P. Mihai, T. Schulz, S.-J. Noh, C. H. Marrows, T. A. Moore, and M. Kläui, Spinorbit torque-driven magnetization switching and thermal effects studied in Ta\CoFeB\MgO nanowires, Appl. Phys. Lett. 105, 122404 (2014).
- [9] K. Garello, C. O. Avci, I. M. Miron, M. Baumgartner, A. Ghosh, S. Auffret, O. Boulle, G. Gaudin, and P. Gambardella, Ultrafast magnetization switching by spin-orbit torques, Appl. Phys. Lett. 105, 212402 (2014).
- [10] M. Cubukcu, O. Boulle, M. Drouard, K. Garello, C. O. Avci, I. M. Miron, J. Langer, B. Ocker, P. Gambardella, and G. Gaudin, Spin-orbit torque magnetization switching of a three-terminal perpendicular magnetic tunnel junction, Appl. Phys. Lett. 104, 042406 (2014).
- [11] S. Woo, M. Mann, A. J. Tan, L. Caretta, and G. S. D. Beach, Enhanced spin-orbit torques in Pt/Co/Ta heterostructures, Appl. Phys. Lett. 105, 212404 (2014).
- [12] O. J. Lee, L. Q. Liu, C. F. Pai, Y. Li, H. W. Tseng, P. G. Gowtham, J. P. Park, D. C. Ralph, and R. A. Buhrman, Central role of domain wall depinning for perpendicular magnetization switching driven by spin torque from the spin Hall effect, Phys. Rev. B 89, 024418 (2014).
- [13] Q. Hao and G. Xiao, Giant spin Hall effect and switching induced by spin-transfer torque in a Co₄₀Fe₄₀B₂₀/MgO structure with perpendicular magnetic anisotropy, Phys. Rev. Appl. 3, 034009 (2015).
- [14] Y. Hung, L. Rehm, G. Wolf, and A. D. Kent, Quasistatic and pulsed current-induced switching with spin-orbit torques in ultrathin films with perpendicular magnetic anisotropy, IEEE Magn. Lett. 6, 1 (2015).
- [15] P. Li, T. Liu, H. Chang, A. Kalitsov, W. Zhang, G. Csaba, W. Li, D. Richardson, A. DeMann, G. Rimal,

- H. Dey, J. S. Jiang, W. Porod, S. B. Field, J. Tang, M. C. Marconi, A. Hoffmann, O. Mryasov, and M. Wu, Spin-orbit torque-assisted switching in magnetic insulator thin films with perpendicular magnetic anisotropy, Nat. Commun. 7, 12688 (2016).
- [16] C. Fang, L. Lu, J. Liu, and L. Fu, Topological semimetals with helicoid surface states, Nat. Phys. 12, 936 (2016).
- [17] T. Kondo, M. Nakayama, R. Chen, J. J. Ishikawa, E.-G. Moon, T. Yamamoto, Y. Ota, W. Malaeb, H. Kanai, Y. Nakashima, Y. Ishida, R. Yoshida, H. Yamamoto, M. Matsunami, S. Kimura, N. Inami, K. Ono, H. Kumigashira, S. Nakatsuji, L. Balents, and S. Shin, Quadratic Fermi node in a 3d strongly correlated semimetal, Nat. Commun. 6, 10042 (2015).
- [18] J. Matsuno, K. Ihara, S. Yamamura, H. Wadati, K. Ishii, V. V. Shankar, Hae-Young Kee, and H. Takagi, Engineering a spin-orbital magnetic insulator by tailoring superlattices, Phys. Rev. Lett. 114, 247209 (2015).
- [19] Y. F. Nie, P. D. C. King, C. H. Kim, M. Uchida, H. I. Wei, B. D. Faeth, J. P. Ruf, J. P. C. Ruff, L. Xie, X. Pan, C. J. Fennie, D. G. Schlom, and K. M. Shen, Interplay of spin-orbit interactions, dimensionality, and octahedral rotations in semimetallic SrIrO₃, Phys. Rev. Lett. 114, 016401 (2015).
- [20] D. Pesin and L. Balents, Mott physics and band topology in materials with strong spin-orbit interaction, Nat. Phys. 6, 376 (2010).
- [21] A. Shitade, H. Katsura, J. Kuneš, X.-L. Qi, S.-C. Zhang, and N. Nagaosa, Quantum spin hall effect in a transition metal oxide Na₂IrO₃, Phys. Rev. Lett. **102**, 256403 (2009).
- [22] X. Wan, A. M. Turner, A. Vishwanath, and S. Y. Savrasov, Topological semimetal and Fermi-arc surface states in the electronic structure of pyrochlore iridates, Phys. Rev. B 83, 205101, (2011).
- [23] W. Witczak-Krempa, G. Chen, Y. B. Kim, and L. Balents, Correlated quantum phenomena in the strong spin-orbit regime, Annu. Rev. Cond. Mat. Phys. 5, 57 (2014).
- [24] A. S. Patri, K. Hwang, H.-W. Lee, and Y. B. Kim, Theory of large intrinsic spin Hall effect in iridate semimetals, Sci. Rep. 8, 8052 (2018).
- [25] T. Nan, T. J. Anderson, J. Gibbons, K. Hwang, N. Campbell, H. Zhou, Y. Q. Dong, G. Y. Kim, D. F. Shao, T. R. Paudel, N. Reynolds, X. J. Wang, N. X. Sun, E. Y. Tsymbal, S. Y. Choi, M. S. Rzchowski, Yong Baek Kim, D. C. Ralph, and C. B. Eom, Anisotropic spinorbit torque generation in epitaxial SrIrO₃ by symmetry design, Proc. Natl. Acad. Sci. 116, 16186 (2019).
- [26] H. Wang, K.-Y. Meng, P. Zhang, J. T. Hou, J. Finley, J. Han, F. Yang, and L. Liu, Large spin-orbit torque observed in epitaxial $SrIrO_3$ thin films, Appl. Phys. Lett. **114**, 232406 (2019).
- [27] A. S. Everhardt, M. DC, X. Huang, S. Sayed, T. A. Gosavi, Y. Tang, C.-C. Lin, S. Manipatruni, I. A. Young, S. Datta, J.-P. Wang, and R. Ramesh, Tunable charge to spin conversion in strontium iridate thin films, Phys. Rev. Mater. 3, 051201 (2019).
- [28] S. Crossley, A. G. Swartz, K. Nishio, Y. Hikita, and H. Y. Hwang. All-oxide ferromagnetic resonance and spin pumping with SrIrO₃, Phys. Rev. B 100, 115163 (2019).
- [29] X. Huang, S. Sayed, J. Mittelstaedt, S. Susarla, S. Karimeddiny, L. Caretta, H. Zhang, V. A. Stoica, T. Gosavi, F. Mahfouzi, Q. Sun, P. Ercius, N. Kioussis, S. Salahuddin, D. C. Ralph, and R. Ramesh, Novel

- spin-orbit torque generation at room temperature in an all-oxide epitaxial La_{0.7}Sr_{0.3}MnO₃/SrIrO₃ system, Adv. Mater. **33**, 2008269 (2021).
- [30] L. Liu, Q. Qin, W. Lin, C. Li, Q. Xie, S. He, X. Shu, C. Zhou, Z. Lim, J. Yu, W. Lu, M. Li, X Yan, S. J. Pennycook, and J. Chen, Current-induced magnetization switching in all-oxide heterostructures, Nat. Nanotech. 14, 939 (2019).
- [31] L. Liu, G. Zhou, X. Shu, W. Li, L. Ren, C. Zhou, T. Zhao, R. Guo, Q. Xie, H. Wang, J. Zhou, P. Yang, S.J. Pennycook, Xu X., and J. Chen, Room-temperature spin-orbit torque switching in a manganite-based heterostructure, Phys. Rev. B 105, 144419 (2022).
- [32] Y. Wang, R. Ramaswamy, M. Motapothula, K. Narayanapillai, D. Zhu, J. Yu, T. Venkatesan, and H. Yang, Room-temperature giant charge-to-spin conversion at the SrTiO₃-LaAlO₃ oxide interface, Nano Lett. 17, 7659 (2017).
- [33] S. Hori, K. Ueda, T. Kida, M. Hagiwara, and J. Matsuno, Spin-orbit torque generation in bilayers composed of CoFeB and epitaxial SrIrO₃ grown on an orthorhombic DyScO₃ substrate, Appl. Phys. Lett. 121, 022402 (2022).
- [34] See supplemental material for detailed information on sample growth, structural characterizations, experimental data, and analyses.
- [35] A. M. Glazer, Simple ways of determining perovskite structures, Acta Crystal. Sec. A 31, 756 (1975).
- [36] L. Liu, T. Moriyama, D. C. Ralph, and R. A. Buhrman, Spin-torque ferromagnetic resonance induced by the spin Hall effect, Phys. Rev. Lett. 106, 036601 (2011).
- [37] C. O. Avci, K. Garello, M. Gabureac, A. Ghosh, A. Fuhrer, S. F. Alvarado, and P. Gambardella, Interplay of spin-orbit torque and thermoelectric effects in ferromagnet/normal-metal bilayers, Phys. Rev. B 90, 224427 (2014).
- [38] Y. Lv, J. Kally, D. Zhang, J. S. Lee, M. Jamali, N. Samarth, and J.-P. Wang, Unidirectional spin-Hall and Rashba-Edelstein magnetoresistance in topological insulator-ferromagnet layer heterostructures, Nat. Commun. 9, 111 (2018).
- [39] Y. Wen, J. Wu, P. Li, Q. Zhang, Y. Zhao, A. Manchon, J. Q. Xiao, and X. Zhang, Temperature dependence of

- spin-orbit torques in Cu-Au alloys, Phys. Rev. B 95, 104403 (2017).
- [40] C. O. Avci, K. Garello, A. Ghosh, M. Gabureac, S. F. Alvarado, and P. Gambardella, Unidirectional spin Hall magnetoresistance in ferromagnet/normal metal bilayers, Nat. Phys. 11, 570 (2015).
- [41] L. Liu, T. Moriyama, D. C. Ralph, and R. A. Buhrman, Spin-torque ferromagnetic resonance induced by the spin Hall effect, Phys. Rev. Lett. 106, 036601, (2011).
- [42] P. Li, L. J. Riddiford, C. Bi, J. J. Wisser, X.-Q. Sun, A. Vailionis, M. J. Veit, A. Altman, X. Li, M. DC, S. X. Wang, Y. Suzuki, and S. Emori, Charge-spin interconversion in epitaxial Pt probed by spin-orbit torques in a magnetic insulator, Phys. Rev. Mater. 5, 064404 (2021).
- [43] A. R. Mellnik, J. S. Lee, A. Richardella, J. L. Grab, P. J. Mintun, M. H. Fischer, A. Vaezi, A. Manchon, E.-A. Kim, N. Samarth, and D. C. Ralph, Spin-transfer torque generated by a topological insulator, Nature 511, 449 (2014).
- [44] L. Zhu, L. Zhu, S. Shi, M. Sui, D.C. Ralph, and R.A. Buhrman, Enhancing spin-orbit torque by strong interfacial scattering from ultrathin insertion layers, Phys. Rev. Appl. 11, 061004 (2019).
- [45] C.-Y. Hu, Y.-F. Chiu, C.-C. Tsai, C.-C. Huang, K.-H. Chen, C.-W. Peng, C.-M. Lee, M.-Y. Song, Y.-L. Huang, S.-J. Lin, and C.-F. Pai, Toward 100% spin—orbit torque efficiency with high spin—orbital Hall conductivity Pt-Cr alloys, ACS Appl. Electron. Mater. 4, 1099 (2022).
- [46] L. Zhu, L. Zhu, and R. A. Buhrman, Fully spintransparent magnetic interfaces enabled by the insertion of a thin paramagnetic nio layer, Phys. Rev. Lett. 126, 107204 (2021).
- [47] L. Wang, K. Shi, S. Peng, K. Cao, H. Yang, J. Gao, W. Zhao, and C. Zhao, Large spin Hall effect of perpendicularly magnetized β-W/CoFeB/MgO layers with high thermal stability, Japn. J. Appl. Phys. 58, 050903 (2019).
- [48] S. Isogami, Y. Shiokawa, A. Tsumita, E. Komura, Y. Ishitani, K. Hamanaka, T. Taniguchi, S. Mitani, T. Sasaki, and M. Hayashi, Spin-orbit torque driven magnetization switching in W/CoFeB/MgO-based type-y three terminal magnetic tunnel junctions, Sci. Rep. 11, 16676 (2021).

Supplementary for large spin-orbit-torque efficiency and room-temperature magnetization switching in $SrIrO_3/Co$ -Fe-B heterostructures

Peng Li,^{1,2} Sanyum Channa,^{1,2} Xiang Li,^{3,4} Laith Alahmed,⁵ Chunli Tang,⁵ Di Yi,¹ Lauren Riddiford,^{1,2} Jacob Wisser,^{1,2} Purnima P. Balakrishnan,^{1,6} Xin Yu Zheng,^{1,2} Di Lu,⁷ Arturas Vailionis,¹ Shan X. Wang,^{3,4} and Yuri Suzuki^{1,2}

 $^{1}Geballe\ Laboratory\ of\ Advanced\ Materials,$

Stanford University, Stanford, California 94305, USA

²Department of Applied Physics, Stanford University, Stanford, CA 94305, USA

³Department of Electrical Engineering,

Stanford University, Stanford, California 94305, USA

⁴Department of Materials Science and Engineering,

Stanford University, Stanford, California 94305, USA

⁵Department of Electrical and Computer Engineering,

Auburn University, Auburn, AL 36849

⁶Department of Physics, Stanford University, Stanford, CA 94305, USA

⁷School of Microelectronics, University of Science and Technology of China, Hefei 230052, China

(Dated: March 30, 2023)

I. SAMPLE GROWTH PROCEDURE

A KrF excimer laser running at 1 Hz and fluence of 1 J/cm² was used to deposit thin films of SrIrO₃ at a distance 4 cm away from the target in an oxygen (O₂) pressure of 50 mTorr and at a growth temperature of 600°C. After the SrIrO₃ deposition, the substrate was cooled down at a rate of 10°C/min in 50 Torr O₂. The CoFeB layer was subsequently sputtered onto SrIrO₃ at 3 mTorr Ar, room temperature and dc power of 15 W in an ion beam sputtering system. A Ta (1.5 nm)/MgO (2 nm) stack was deposited onto the structure to prevent CoFeB oxidation.

II. SPIN-TORQUE FERROMAGNETIC RESONANCE

As illustrated in Fig. 2a, as-deposited SrIrO₃/CoFeB(4)/MgO(2)/Ta(2) (all numbers in parenthesis hereafter are in the unit of nm) stacks on LSAT substrates were patterned into 40 μ m-wide and 60 μ m long microstrips. The microwave current induces an oscillating transverse spin current in the SrIrO₃ layer. This spin current is injected into the CoFeB layer exciting spin precession and generating an RF anisotropic magnetoresistance. This magnetoresistance, rectified with the microwave current, generates a dc voltage. The ST-FMR spectra in Fig. 2b are obtained by sweeping external in-plane magnetic fields through the CoFeB resonance condition on a CoFeB (5 nm) /SrIrO₃ (12.9 nm) sample at different frequencies. The amplitude decreases at higher frequencies due to increased impedance in the microwave circuit. The STFMR lineshapes can be fitted with symmetric and asymmetric Lorentzian functions, F_s and F_a , in the form of $V = V_s F_s + V_a F_a$.

III. ELECTRICAL MEASUREMENT

The electrical measurement set up is shown in Figures 3(a) and (b) with the current source connected longitudinally (along the x-axis) and the voltmeter connected to either the longitudinal (x) or transverse (y) terminals for R_{xx} and R_{xy} measurements, respectively. When an ac current flows in the device, oscillating SOTs are generated, giving rise to first and second harmonic resistances. When a 2 T magnetic field is applied to saturate the CoFeB layer and is rotated within the xy-plane, the first and second harmonic transverse resistances $R_{xy-1\omega}$, $R_{xy-2\omega}$ can be expressed by the following equations:

$$R_{\text{xv-1}\omega} = R_{\text{AHE}}cos(\theta) + R_{\text{PHE}}sin^2(\theta)sin(2\phi) \tag{1}$$

$$R_{\text{xy-}2\omega} = \frac{1}{2} \left(R_{\text{AHE}} \frac{H_{\text{DL}}}{H + H_{\text{Demag}} - H_k} + R_{\Delta \text{T}} \right) \cos(\phi) + R_{\text{PHE}} \frac{H_{\text{FL}} + H_{\text{Oe}}}{H} \cos(2\phi) \cos(\phi) \quad (2)$$

where $R_{\rm AHE}$, $R_{\rm PHE}$ and $R_{\Delta T}$ are the anomalous Hall, planar Hall and thermal resistances, respectively. The thermal resistances originate from the anomalous Nernst effect (ANE) and the spin Seebeck effect (SSE). $H_{\rm DL}$, $H_{\rm FL}$, $H_{\rm Oe}$ are the damping-like, field-like and oersted fields, respectively. $H_{\rm Demag}$ and H_k are the demagnetizing and anisotropy fields of CoFeB. It should be noted that θ is the angle of magnetization with respect to the out-of-plane direction, and ϕ is the angle of magnetization with respect to the current axis (x-axis).

IV. FILM RESISTIVITY

Below is the temperature dependent resistivity of single layer films of CoFeB and $SrIrO_3$ on LSAT substrates.

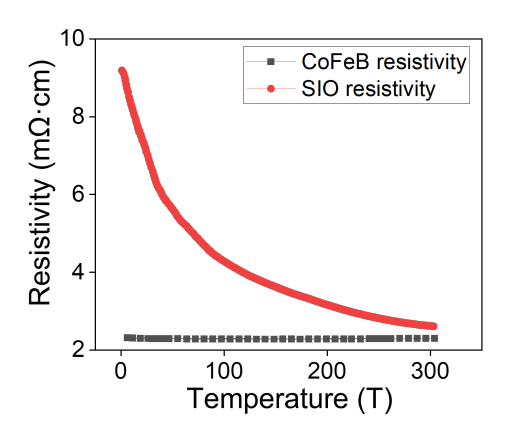


FIG. S1. Temperature dependence of SrIrO₃ (10.8 nm) and CoFeB (5 nm) resistivity

V. FIRST HARMONIC OF R_{xy}

The first harmonic Hall resistance $R_{xy-1\omega}$ shows a typical planar Hall effect, which is well fitted by $sin^2(\theta)sin(2\phi)$ where $\theta=90^o$ as shown in Fig. S2.

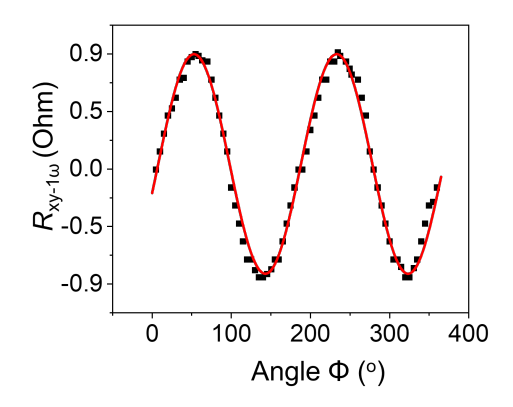


FIG. S2. Angular dependence of the first harmonic Hall resistance $R_{xy-1\omega}$.

VI. FIELD-LIKE TORQUE CONTRIBUTION

We have plotted the $R_{xy-2\omega-FL}$ vs. $1/H_{ext}$ as Fig. S3. As one can see, it is almost a flat line. It can be calculated using Slope/ R_{PHE} , which is 0.09 Oe.

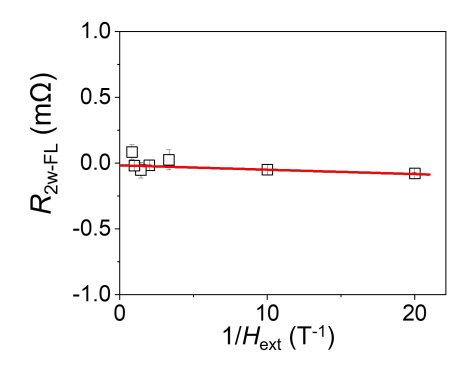


FIG. S3. $R_{xy\text{-}2\omega\text{-}FL}$ vs. $1/H_{\rm ext}$ fitted by a straight line.